CRYSTAL GROWTH & DESIGN

pubs.acs.org/crystal

Article

Effect of Nucleotides on the Phase and Crystal Structure of Synthetic Calcium Carbonate

Arad Lang, Iryna Polishchuk, Alexander Katsman, and Boaz Pokroy*

Cite This: *Cryst. Growth Des.* 2023, 23, 5117−5125

Read Online

ACCESS | Metrics & More | Article Recommendations | Supporting Information

ABSTRACT: The interactions of organic hereditary materials (*i.e.*, DNA and RNA) with inorganic minerals are of key importance in many fields of research, from archeology and paleontology to medicine. It was previously shown that the building blocks of the main structural biomacromolecules, amino acids and monosaccharides, can be incorporated into the crystal lattice of calcium carbonate ($CaCO_3$), the most abundant biomineral. Here, we continue this reductionist approach and study how the mineral host is affected when grown in the presence of mono- or triphosphate nucleotides—the building blocks of nucleic acids. We show that the nucleotides facilitate the stabilization of the amorphous polymorph of $CaCO_3$, as well as promote the formation of vaterite, its least thermodynamically stable anhydrous crystalline phase. We use high-resolution powder X-ray diffraction, and a variety of chemical analysis tools, to demonstrate the mechanism by which nucleotides become incorporated within the vaterite lattice.

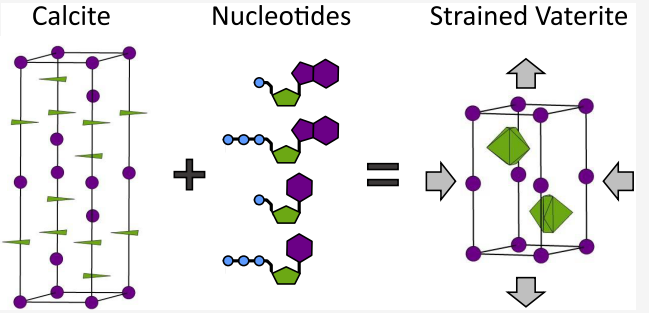

INTRODUCTION

Calcium carbonate ($CaCO_3$) is the most abundant biomineral.[1] While geological calcite is considered to be brittle, its biogenic counterpart can be much harder and tougher.[2,3] Living organisms achieve this improvement in mechanical properties by various strategies, one of which is by means of additives, which are incorporated into the $CaCO_3$ lattice and therefrom induce internal stresses, hence hindering cracks from propagating.[4] The available additives for the organisms to use can be divided into two groups: (i) inorganic additives, usually divalent metal cations, substituting for Ca^{+2},[5−8] and (ii) organic additives, in the form of proteins and polysaccharides, occluded inside the biomineral structure.[9−13]

The field of bio-inspired crystal growth encompasses research that aims at developing novel materials using strategies found in Nature.[14,15] In the realm of $CaCO_3$, efforts were made to understand the impact of various crystallization conditions and additives on the resulting structure, shape, and physical properties of the crystals. For the last decade, our group,[16−20] as well as others,[5,21−29] have shown that calcite and vaterite, two of the anhydrous polymorphs of $CaCO_3$, can incorporate both organic and inorganic additives. Specifically, it was demonstrated that the building blocks of proteins and polysaccharides, namely, amino acids (AAs)[16,29,30] and monosaccharides (MSs),[19] respectively, can be incorporated into the crystal lattice of the host, and induce changes in its lattice parameters. For both AAs and MSs, it was proven that the carboxylic (acidic) moiety plays a key role in the incorporation process. Such incorporation was shown to induce changes in the crystal structure,[17,30] morphology,[17,19] thermal expansion coefficient,[17] and mechanical properties[30] of the $CaCO_3$ host.

Although they do not embrace any structural role, the significance of nucleic acids (NAs: DNA and RNA) as biomacromolecules is undeniable, as they encode the genetic information of all living organisms.[31] The interaction of DNA and DNA-like molecules with different minerals was deeply studied over the years. It was shown that DNA can be adsorbed on the surface of natural minerals, mostly hydroxyapatite[32−35] and clay.[36,37] The adsorption can induce NAs polymerization,[38,39] as well as provide protection from the natural degradation of the NAs over time.[40−44] Some researchers even dared to correlate nucleotide−mineral interactions with the origin of life.[45−47] Moreover, the presence of extracellular DNA, and even individual nucleotides, was shown to have an effect on mineral formation.[48−50] As for the interaction of NAs with synthetic $CaCO_3$, it was mainly studied for purposes of controlled gene delivery.[51−54] Moreover, it was shown that the presence of DNA during $CaCO_3$ synthesis enables controlling the morphology of the resulting calcite microcrystals[55−57] and inhibits its growth.[58,59]

Received: March 26, 2023
Revised: May 15, 2023
Published: June 9, 2023

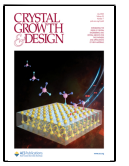

https://doi.org/10.1021/acs.cgd.3c00367
Cryst. Growth Des. 2023, 23, 5117−5125

In this work, we aim to study how the structure of synthetic $CaCO_3$ is affected when grown in the presence of the building blocks of NAs, namely, nucleotides. Do they solely affect the microstructure and morphology or rather also the polymorph? Do they get incorporated into the crystal host lattice? To this end, we selected a nucleotide of each type of nucleobase: adenosine (a purine, which creates two hydrogen bonds in DNA) and cytosine (a pyrimidine, which creates three hydrogen bonds in DNA).[60] Moreover, to study the effect of the phosphate moiety of the nucleotide, for each case, we used both mono- and triphosphate derivatives.

RESULTS AND DISCUSSION

We synthesized $CaCO_3$ in the presence of two nucleobases, adenosine and cytosine, chemically linked to a ribose ring and one or three phosphate groups. The $CaCO_3$ samples were grown in the presence of three different concentrations (1, 5, 10 mM), of four different nucleotides: adenosine monophosphate (AMP), adenosine triphosphate (ATP), cytosine monophosphate (CMP), and cytosine triphosphate (CTP, see Figure S1 for chemical structures, and the Experimental Section for more details).

Our first objective was to determine whether the presence of nucleotides during $CaCO_3$ precipitation results in their incorporation into the mineral's structure. To this end, we used inductively coupled plasma optical emission spectroscopy (ICP-OES) to detect phosphorus. These measurements were performed only after a bleaching treatment, which allows us to assume that the phosphorus detected within the samples originates solely from incorporated organic molecules, rather than from molecules adsorbed on the crystal surface (see the Experimental Section for more information). The concentration of the nucleotide molecules in the crystals was calculated according to eq 1

$$[\mathrm{Nuc}]_{\mathrm{cryst}} = \frac{[\mathrm{P}]}{[\mathrm{Ca}]} \times \frac{1}{N_{\mathrm{P}}} \quad (1)$$

where [P] and [Ca] are the measured concentrations of phosphorus and calcium, respectively (in M), and N_P is the number of P atoms in the nucleotide (N_P = 1 for AMP and CMP, and N_P = 3 for ATP and CTP).

As presented in Figure 1a, the concentration of nucleotides within the crystals monotonically increases with the increase in their amount added to the crystallization solution. The correlation between the ICP-OES results and the quantification of nitrogen atoms, as was performed using CHNS analysis (Figure 1b), proves that the measured signal of P atoms indeed arises from the nucleotide molecules, rather than from decomposed (inorganic) phosphate anions, if any. It is worth mentioning that the variation in the measured nucleotide concentration in each sample can stem from their inhomogeneity (each sample contains up to three different polymorphs, as will be shown later). This is even more pronounced due to the low sampling volumes required for ICP-OES and CHNS analyses. Considering that nucleotide molecules contain different amounts of phosphate groups, it becomes evident that those possessing three phosphates (ATP and CTP) are incorporated at a higher level than that of the monophosphate molecules (AMP and CMP). Moreover, when comparing molecules with different nucleobases, one can conclude that the adenosine-based molecules are incorporated at higher levels than that of the cytosine-based ones.

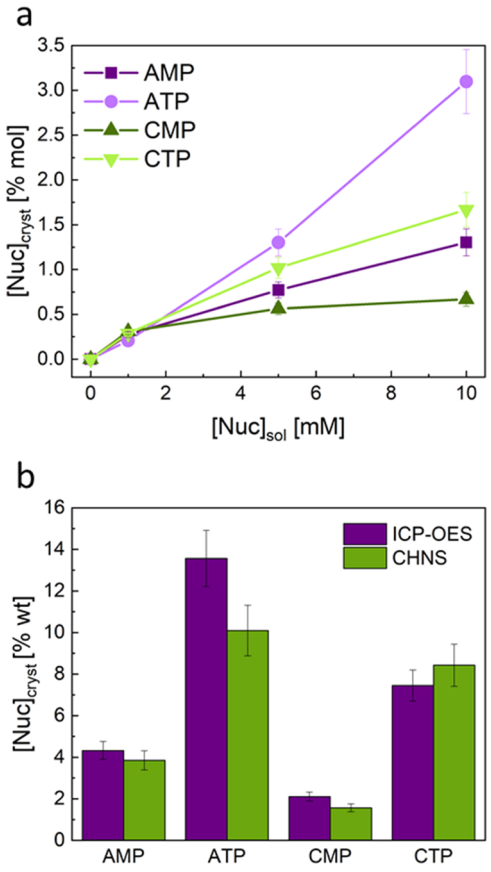

Figure 1. Chemical analysis of $CaCO_3$ crystals grown in the presence of selected nucleotides: (a) Concentration of nucleotides within the crystals based on ICP-OES, as a function of nucleotides concentration in the crystallization solution. (b) Comparison between the concentration of occluded nucleotides measured by ICP-OES and CHNS analyses. These results were obtained for crystals grown with $[\mathrm{Nuc}]_{\mathrm{sol}}$ = 10 mM.

As $CaCO_3$ can be found in several crystalline phases,[61,62] we were interested to investigate whether the addition of nucleotides influences its polymorph selection. To this end, we employed high-resolution powder X-ray diffraction (HR-PXRD). Figure 2 presents HR-PXRD patterns collected from samples grown in the presence of different nucleotides in solution. It is clear that as the concentration of nucleotides increases in the solution, the amount of vaterite formed increases. In the case of the highest concentration of ATP and CTP (10 mM), vaterite is the predominant polymorph that forms (98 wt %).

Figure 2b confirms that the relative amount of vaterite increases with the concentration of added nucleotides (for full and indexed diffractograms, refer to Figure S2). We believe that this case corroborates previous reports, in which negatively charged organic molecules, when added to the precipitation solution of $CaCO_3$, were shown to stabilize vaterite.[63−68] It should be noted that the presence of nucleotides during precipitation induces a reduction in its crystallinity. The latter can be concluded from the observation that the background signal of the diffraction patterns, and especially the broad diffraction peak at low 2θ angles, intensifies with an increase in the amount of ATP and CTP (Figure S3). Broad diffraction peaks of this sort are known to attest the presence of amorphous materials, specifically

https://doi.org/10.1021/acs.cgd.3c00367
Cryst. Growth Des. 2023, 23, 5117−5125

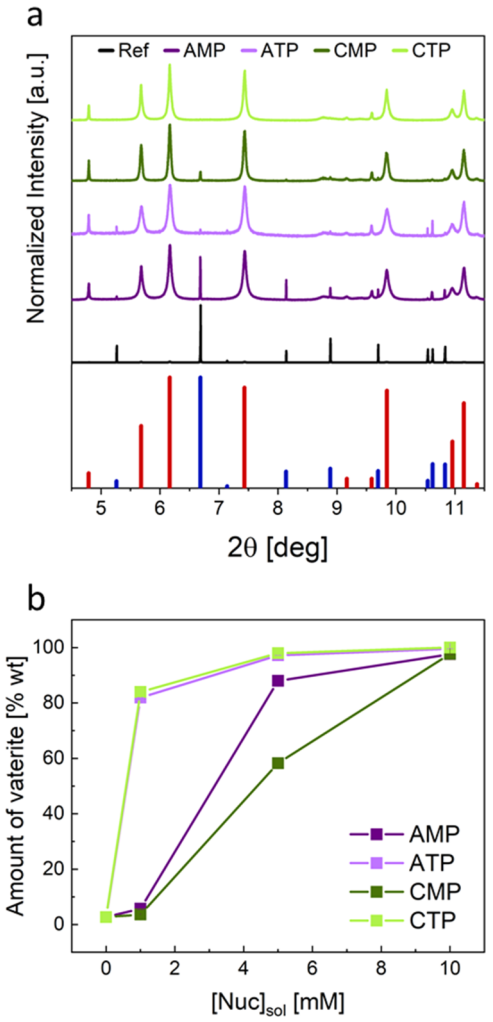

Figure 2. Phase analysis of $CaCO_3$ crystals grown from solutions containing nucleotides: (a) HR-PXRD patterns (λ = 0.3542 Å), showing the crossover from calcite to vaterite stabilization with the addition of nucleotides. The blue and red lines at the bottom represent the theoretical reflections of calcite (ICDD card #00-005-0586) and vaterite (ICDD card #00-060-0483), respectively. (b) Relative amount of vaterite as a function of nucleotide concentration in crystallization solution calculated *via* Rietveld refinement.

amorphous calcium carbonate (ACC).[69−71] The presence of ACC was further confirmed using Fourier transform infrared (FT-IR) spectroscopy. As presented in Figure 3, both the stretching (ν) and bending (δ) characteristic bands of the O−H bonds, as well as the shoulder in the ν_3 band of $CaCO_3$, appear in the spectrum of the nucleotides-incorporated samples and are absent in that of the reference sample (Figure 3). The latter three IR bands are commonly characteristic of ACC.[72] Moreover, due to the formation of vaterite, the ν_3 band is slightly shifted to a higher wavenumber in the case of the samples containing nucleotides (compared to the reference sample).[73] The stabilization of ACC is known to prevail when organic additives,[71,74−76] and, in particular, phosphate-rich species,[77,78] are introduced.

Since vaterite is the major phase among the resulting $CaCO_3$ polymorphs (Figure 2), we further studied how the incorporation of nucleotides (Figure 1) affects its crystalline structure. Although the exact structure of vaterite is still a matter of debate,[79−81] it is established that its substructure,

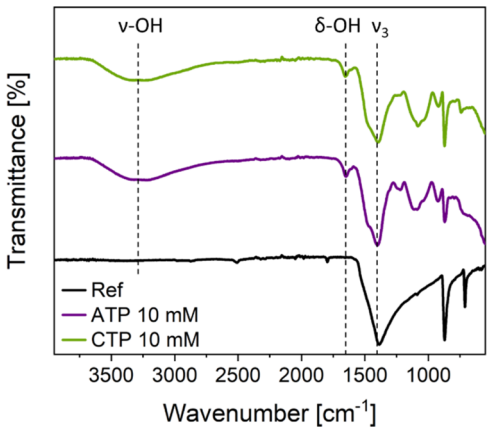

Figure 3. FT-IR spectra of selected samples demonstrating the presence of ACC in the nucleotide-incorporated samples solely. Bands relevant to ACC are labeled.

which is responsible for the majority of its Bragg reflections, possesses a hexagonal unit cell, with lattice parameters of $a \approx 4.1$ Å and $c \approx 8.5$ Å.[79]

We calculated the lattice distortions in our samples by comparing the lattice parameters of the nucleotide-incorporated samples with those of the control samples (grown without the addition of nucleotides to the solution), extracted from the HR-PXRD measurements using Rietveld refinement (Table S1), and according to eq 2

$$\frac{\Delta a}{a} = \frac{a_N - a_C}{a_C}, \quad \frac{\Delta c}{c} = \frac{c_N - c_C}{c_C} \tag{2}$$

where a_N and c_N are the lattice parameters of the nucleotide-incorporated samples, and a_C and c_C are those of the control samples, respectively (which also contained small amounts of vaterite—2.706% wt, as was calculated using Rietveld refinement).

The calculated lattice distortions are presented in Figure 4. While the distortions along the *a* and *c* directions are similar in magnitude, they are opposite in sign: the incorporation of nucleotides induces a contraction of the *a*-parameter (Figure 4a), and an elongation of the *c*-parameter (Figure 4b). Apparently, different nucleotides demonstrate a similar behavior trend, *i.e.*, the magnitude of the induced lattice distortions depends on the amount of the incorporated nucleotide, rather than on its molecular structure. This trend is demonstrated in Figure S4, where the (100) reflection, which represents the *a*-parameter, is shown to shift to higher 2θ values (corresponding to a smaller *d*-spacing).[82] On the contrary, the (002) reflection, which represents the *c*-parameter, shifts to lower 2θ values (corresponding to a higher *d*-spacing). Upon heating (300 °C for 3 h, under an ambient atmosphere), the organics degrade[16] and the induced strains relax (Figure S6a,b). Moreover, partial crystallization of the ACC occurs as well, as the background of the diffraction patterns decreases, while the intensity of the (104) reflection of calcite increases at its expense (Figure S6c,d).

We used high-resolution scanning electron microscopy (HR-SEM) to observe the morphology of the crystals. Figure 5 presents the resulting HR-SEM micrographs. Without any additives, the crystals exhibit the characteristic rhombohedral morphology of calcite.[17,19,30] When nucleotides are added, the spherical morphology of vaterite appears in the shape of the crystals.[18] Furthermore, employing energy-dispersive spectros-

https://doi.org/10.1021/acs.cgd.3c00367
Cryst. Growth Des. 2023, 23, 5117−5125

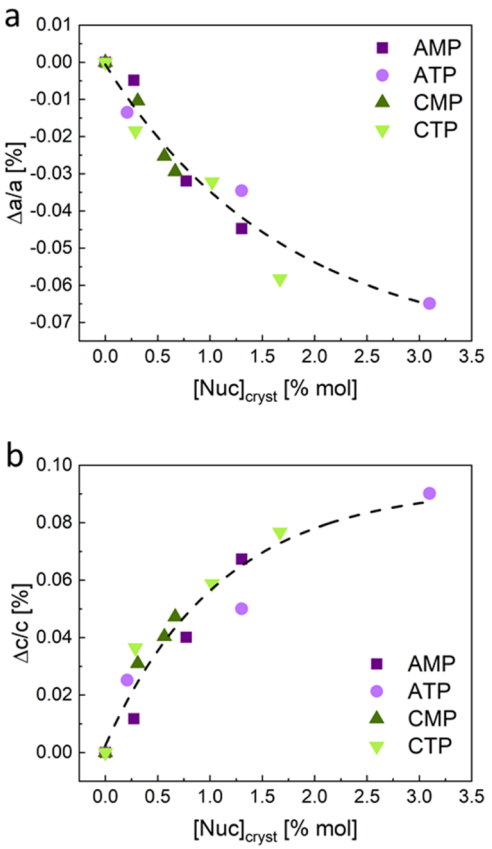

Figure 4. Structural changes in nucleotides-incorporated vaterite crystals. Lattice distortion along the (a) *a*-parameter and (b) *c*-parameter of vaterite, calculated using Rietveld refinement. Dashed black lines represent the general trend.

copy (EDS) in the SEM confirmed that P atoms can indeed be detected within the vaterite crystals (Figure S8). It can be also seen that the crystal size is smaller in the case of the AMP- and CMP-incorporating samples, and even further reduced when ATP and CTP are incorporated. This reduction in crystallite size is confirmed when calculating the coherence length of the samples by fitting the (101) diffraction peak of each sample to a Voigt function (see Figure S5).[10,83] Figure 5, as well as the low-magnification micrographs in Figure S9, reveals that the nucleotide-incorporated samples appear with two different morphologies—micron-sized spheres and nano-sized aggregates with no definite shape. These morphologies are characteristic of vaterite[18] and ACC,[71] respectively, as we also confirmed using Raman spectroscopy (Figure S7).

To further confirm the incorporation of nucleotides, as well as to study the thermal behavior of the crystals, we employed thermogravimetric analysis (TGA, Figure 6). As expected, the

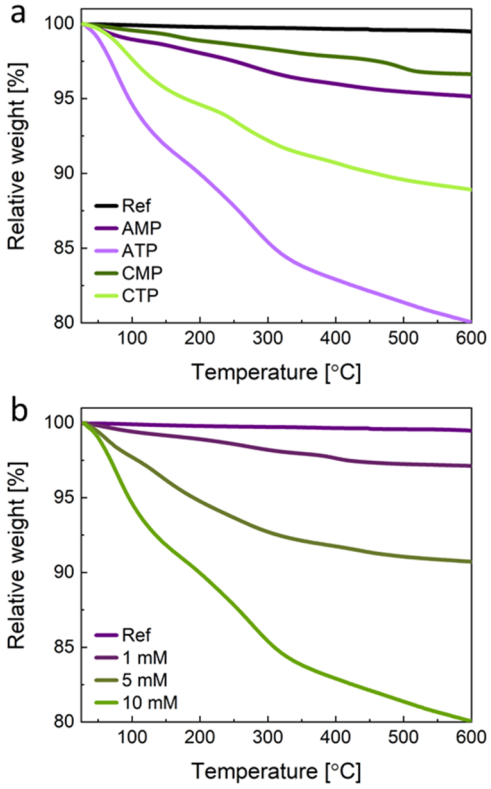

Figure 6. Thermal analysis of the nucleotides-$CaCO_3$ crystals: TGA curves of (a) samples with the same amount ($[Nuc]_{sol}$ = 10 mM) of different nucleotides in solution and (b) samples with different amounts of the same nucleotide (ATP).

weight of the nucleotides-incorporated samples decreases upon heating up to 600 °C, while for the reference sample, it remains rather constant. These results support our previous conclusion that the organic nucleotide molecules are indeed incorporated into the $CaCO_3$ structure. A greater weight loss is observed in the case of incorporation of triphosphates (compared to monophosphates), and in the case of adenosine (as compared to cytosine, Figure 6a). Moreover, a higher concentration of incorporated nucleotide molecules results in a larger weight loss upon heating (Figure 6b).

It can be noted that the total weight loss can be generally assigned to the two main contributions: (*i*) decomposition of the incorporated organic molecules and (*ii*) water evaporation,

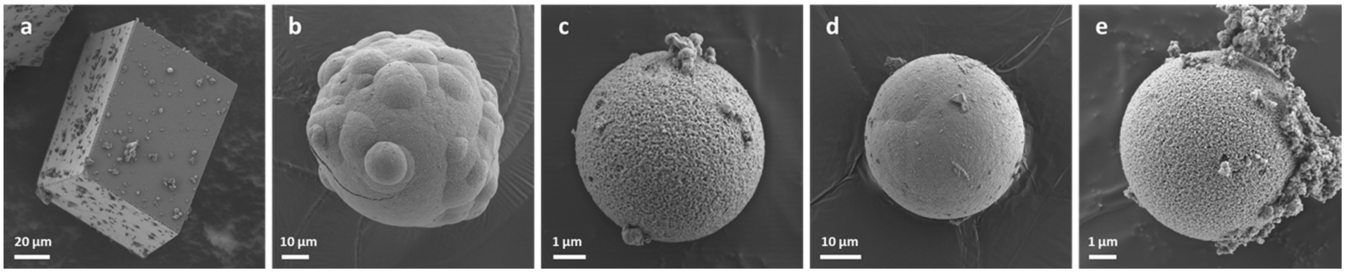

Figure 5. HR-SEM micrographs of (a) control sample and nucleotide-incorporated samples ($[Nuc]_{sol}$ = 10 mM): (b) AMP, (c) ATP, (d) CMP, (e) CTP.

https://doi.org/10.1021/acs.cgd.3c00367
Cryst. Growth Des. 2023, 23, 5117−5125

originating solely from the ACC phase.[84] In our case, the samples lose their weight upon heating due to the two main events (see Figure S10 for the derivatives of the plots). The first event occurs at around 100−150 °C and is ascribed to the evaporation of water from the surface of the crystals as well as structural water from the ACC. The second event, at 200−300 °C, can be attributed to the decomposition of organics.

We further attempted to understand the mechanism by which nucleotides get incorporated within the vaterite unit cell during crystallization. Considering the synthesis procedure, we can assume that when the nucleotides are set to dissolve in a Ca^{+2}-containing solution, dissolved Nuc-Ca ion (pre-nucleation) clusters can be formed due to the strong phosphate−calcium coulombic interaction.[85,86] While in the case of AMP and CMP the phosphate−Ca interaction is relatively weak, a significant complexation of Ca^{+2} may occur in the case of ATP and CTP.[87−89] A stronger phosphate−Ca binding could explain the elevated levels of incorporation in the case of triphosphate molecules (Figure 1). In addition, the Nuc-Ca ion clusters may act as nucleation sites for the formation of ACC, which later may transform into vaterite. Further, the transformation of the vaterite into calcite is inhibited by the presence of the phosphate groups of the nucleotide molecules.[90]

Akin to the incorporation of aspartic acid[30] and acidic monosaccharaides[19] into calcite, which was shown to be facilitated *via* their carboxylic moiety,[19] it is reasonable to assume that the incorporation of nucleotides into vaterite occurs *via* substitution of a negatively charged phosphate group for a carbonate anion in vaterite. It was indeed shown in the past that single (inorganic) phosphate anions can be incorporated into calcite[91,92] and vaterite.[93] According to Kennard et al.,[76] the distance between two oxygen atoms in ATP, which are connected to the same phosphate (O*i*-O*ii*, i = 1,2,3), is approximately 2.495 Å.[94] The Ca−O bond lengths in vaterite vary in the range of 2.26−2.9 Å.[61] By adding two Ca−O bonds, we obtain a Ca−Ca distance of the Ca-O*i*-P-O*ii*-Ca chain varying in the range L_{Ca-Ca} = 7.015−8.295 Å. This distance is somewhat shorter than the Ca−Ca distance along the [$\bar{2}$21] crystallographic direction in vaterite ($L_{[\bar{2}21]}$ = 8.315 Å). Hence, such incorporation should induce macroscopic strain of the lattice. In particular, it can result in a lattice shrinkage caused by contraction of the *a*-axis, accompanied with the elongation of the *c*-axis (see Figure 7 showing a schematic representation, and Figure S11 presenting the unit cell volumes). Calculations of elastic strains induced by the incorporation of nucleotides and the resulting lattice distortions showed that the nucleotide-incorporating vaterite crystals undergo an internal equiaxial tensile stress of ∼30 MPa (see Supporting Information). Given that the atomic packing factor of vaterite is only ∼50.3%,[95,96] we envisage that the organic moiety of the nucleotides (*i.e.*, the ribose ring and the nucleobase) is interstitially occluded, while the total unit cell volume is reduced due to the phosphate−Ca interactions (Figure S10). This occlusion behavior warrants an answer as to why the concentration of incorporated ATP is higher than of that CTP (and similarly, AMP is higher than that of CMP, see Figure 1), even though the adenosine molecule is bigger in size than cytosine (Figure S1). One possible reason for this is the folding ability of ATP, shown to occur both in the solid state[94] and in solution.[97] CTP, on the other hand, contains a double-bonded oxygen atom on its cytosine ring, which electrostatically repels the phosphate group(s). Hence, CTP is less likely to fold compared to ATP (and the same for AMP as compared to CMP), which makes AMP and ATP fit better within the free space of the vaterite unit cell. Note that more advanced calculative tools are required in order to decipher this hypothesis.

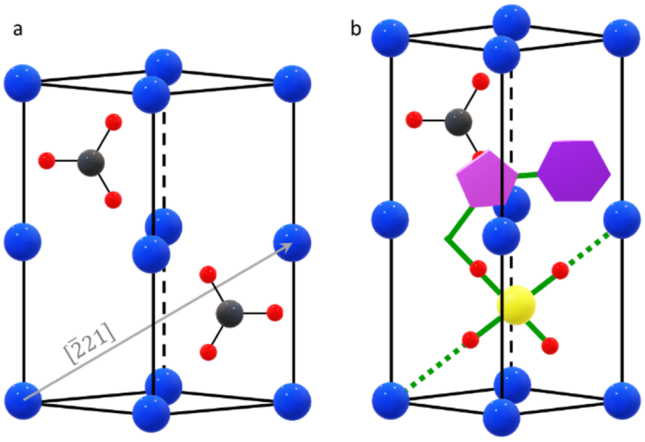

Figure 7. Schematic representation of the vaterite unit cell (a) before, and (b) after the incorporation of a nucleotide molecule. Color legend: blue, Ca; black, C; red, O; yellow, P; purple, ribose and nucleobase rings. The covalent bonds of the nucleotide molecules and the Ca−O interactions are marked with solid and dashed green lines, respectively. The orientation of the carbonate anions was randomly chosen.

CONCLUSIONS

This study represents a thorough investigation of the interaction of nucleotides with $CaCO_3$ mineral. We showed that the presence of nucleotides during $CaCO_3$ growth promotes the formation of both ACC and vaterite—two of its metastable forms. While the effect of nucleotides on the resulting $CaCO_3$ polymorph was recently shown,[68] in this current study, we proved for the first time, *via* HR-PXRD, that the nucleotides can get incorporated into the vaterite crystal lattice, and induce anisotropic lattice strain. This strain is manifested by an expansion along the *c*-axis and a contraction along the *a*-axis of the hexagonal vaterite unit cell. The level of incorporation depends on the molecular structure of the incorporated nucleotides: ATP, which contains an adenine nucleobase and three phosphate groups, was incorporated at the highest level (>3%mol). However, the lattice distortions induced by the incorporation depend solely on the concentration of the nucleotides, rather than their structure. Finally, we suggested a mechanism by which the nucleotide-incorporating vaterite crystals form. According to this model, pre-nucleation Nuc-Ca clusters form in the solution and initiate the formation of ACC. This amorphous phase further transforms into metastable vaterite, whose further transformation to the thermodynamically stable calcite is inhibited by the presence of the negatively charged phosphate moieties.

We believe this research can shed light on the complicated organic−inorganic interactions in living organisms, and specifically, on the synergy between biominerals and hereditary materials. It can explain the mechanism by which nucleic acids are preserved, probably *via* incorporation within minerals, along with the effect of mineralization inhibition which occurs due to extracellular nucleotides. Moreover, the results presented in this study may open new routes for gene delivery applications *via* $CaCO_3$ as a mineral hosting nucleic acids.

https://doi.org/10.1021/acs.cgd.3c00367
Cryst. Growth Des. 2023, 23, 5117−5125

EXPERIMENTAL SECTION

Calcium Carbonate Precipitation. A 0.2 M Ca^{+2} stock solution was prepared by dissolving calcium chloride dihydrate ($CaCl_2$*$2H_2O$, Spectrum) in DI water. 50 ml of the solution was transferred to a 100 ml glass beaker, and the required amount of nucleotide (0, 1, 5, 10 mM) was added to the beaker and stirred for complete dissolution. The nucleotides used were adenosine 5′-monophosphate 99% (AMP, Acros Organics), adenosine triphosphate 95% (ATP, Angene), cytidine 5′-monophosphate disodium salt 99% (CMP, Alfa Aesar), and cytidine 5′-triphosphate disodium salt 97% (CTP, Alfa Aesar). Control (reference) samples were prepared the same way, without adding nucleotides to the Ca^{+2} solution. The beakers were covered with Parafilm with 3 holes in it and placed in a sealed desiccator, together with ∼5 g of ammonium carbonate ($(NH_4)_2CO_3$, Sigma-Aldrich), for 1 week. During this time, the $(NH_4)_2CO_3$ spontaneously decomposes according to

$$(NH_4)_2CO_{3(s)} \rightarrow 2NH_{3(g)} + H_2O_{(l)} + CO_{2(g)} \quad (3)$$

Then, the formed CO_2 diffuses into the aqueous solution and initiates $CaCO_3$ precipitation

$$Ca^{+2}_{(aq)} + CO_{2(g)} + H_2O_{(l)} \rightarrow CaCO_{3(s)} + 2H^{+}_{(aq)} \quad (4)$$

After 1 week, the resulting powder samples were filtrated, washed several times with DI water, and left to dry in air.

Samples Bleaching. A small amount of each sample was transferred to an Eppendorf tube. Then, ∼1 mL of sodium hypochlorite solution (NaOCl, ∼5%, Alfa Aesar) was added, and the tube was sealed and shaken for one minute. This way, the organic molecules on the surface of the crystal decompose, and the incorporated ones are not affected. Then, the tubes were centrifuged (10 000 rpm, 10 min) and the liquid was disposed of. This process was repeated three more times with DI water and then once with ethanol in order to remove all NaOCl residue. Then, the samples were left to dry overnight in a vacuum oven at 50 °C.

Phosphorus (P) Determination. P atoms were determined by inductively coupled plasma optical emission spectroscopy (ICP-OES), using an iCAP 6300 Duo ICP-OES spectrometer (Thermo Scientific) for elemental analysis. The dry bleached samples were dissolved in <3% HNO_3 solution (in DI water) and were measured using ICP-OES for the detection of Ca and P.

Nitrogen (N) Determination. N atoms were determined by CHNS Elemental analysis, using a Flash 2000 Organic elemental analyzer (Thermo Scientific). Around 2 mg of each bleached sample was weighed together with 8−10 mg of vanadium (V) in a tin (Sn) crucible and was inserted into the CHNS analyzer. The combustion temperature was set to 950 °C, the carrier gas was He (99.999%), and the flow rate was 140 mL min^{-1}. Combustion was initiated by adding oxygen gas (O_2) at 250 mL min^{-1}, for 5 s.

High-Resolution Powder X-ray Diffraction. HR-PXRD was performed in the European Synchrotron Radiation Facility (ESRF, Grenoble, France).[98] Each powder sample was finely ground and was filled inside a borosilicate capillary (0.5 mm in diameter). The capillary was sealed using wax and mounted on a brass holder. Each sample was scanned using radiation with a wavelength of 0.3542 Å. To accurately determine lattice parameters and microstructural features, Rietveld refinement[99,100] was used, using the GSAS-II software.[101]

Fourier Transform Infrared Spectroscopy. FT-IR spectroscopy was performed using a Thermo Scientific Nicolet iS50 spectrometer, as a few milligrams of each selected sample were scanned in the wavenumbers range of 500−4000 cm^{-1}.

Raman Spectroscopy. A small amount of each selected sample was dispersed on a microscope glass slide and was placed in a LabRAM HR Evolution Micro-Raman. For each sample, the area of interest was selected using an optical microscope, then scanned in the range of 100−1500 cm^{-1}, using a 532 nm laser.

High-Resolution Scanning Electron Microscopy. HR-SEM micrographs were taken using a Zeiss Ultra+ FEG-SEM. The energy of the primary electrons was set to 1.5 keV.

Energy-Dispersive Spectroscopy. EDS was performed in the Ultra+ SEM. Samples were carbon coated prior to the measurement to avoid electrical charging. From each sample, spectra were taken at three different points.

Coherence Length Calculation. The (101) diffraction peak (the most intense reflection of vaterite) of the selected samples was fitted to a Voigt function using the OriginLab software. Then, the coherence length was calculated based on the Lorentzian portion (W_L) of the diffraction peak full width at half-maximum (FWHM).[10,83]

Thermal Analysis. Thermogravimetric analysis (TGA) was performed using a Mettler Toledo TGA/DSC 3+ instrument. 10−20 mg of each sample was transferred to an alumina crucible, which was placed in the instrument. The weight of each sample was recorded in the range of 25−600 °C, as the heating rate was set to 10 °C min^{-1}.

ASSOCIATED CONTENT

Supporting Information

The Supporting Information is available free of charge at https://pubs.acs.org/doi/10.1021/acs.cgd.3c00367.

Full HR-PXRD patterns and Rietveld refinement results, chemical structures, and full crystallization model calculations (PDF)

AUTHOR INFORMATION

Corresponding Author

Boaz Pokroy − *Department of Materials Science and Engineering and The Russell Berrie Nanotechnology Institute, Technion − Israel Institute of Technology, 32000 Haifa, Israel; The Nancy and Stephen Grand Technion Energy Program, Technion − Israel Institute of Technology, Haifa 3200003, Israel;* orcid.org/0000-0003-0480-7250; Email: bpokroy@technion.ac.il

Authors

Arad Lang − *Department of Materials Science and Engineering and The Russell Berrie Nanotechnology Institute, Technion − Israel Institute of Technology, 32000 Haifa, Israel;* orcid.org/0000-0003-3692-7628

Iryna Polishchuk − *Department of Materials Science and Engineering and The Russell Berrie Nanotechnology Institute, Technion − Israel Institute of Technology, 32000 Haifa, Israel*

Alexander Katsman − *Department of Materials Science and Engineering and The Russell Berrie Nanotechnology Institute, Technion − Israel Institute of Technology, 32000 Haifa, Israel*

Complete contact information is available at: https://pubs.acs.org/10.1021/acs.cgd.3c00367

Notes

The authors declare no competing financial interest.

ACKNOWLEDGMENTS

We thank the European Synchrotron Radiation Facility (ESRF, Grenoble, France) for provision of synchrotron radiation facilities and we would like to thank Dr. Catherine Dejoie for assistance and support in using beamline ID22. B.P. acknowledges the Technion Human Health Initiative (THHI) Collaborative Research Project Grant No. 905150. A.L. acknowledges financial support from the Israeli Ministry of Energy, as part of the scholarships program for M.Sc. and Ph.D. students.

REFERENCES

(1) Lowenstam, H. A.; Weiner, S. *On Biomineralization*; Oxford University Press: Cary, 1989.
(2) Chen, P. Y.; Lin, A. Y. M.; Lin, Y. S.; Seki, Y.; Stokes, A. G.; Peyras, J.; Olevsky, E. A.; Meyers, M. A.; McKittrick, J. Structure and Mechanical Properties of Selected Biological Materials. *J. Mech. Behav. Biomed. Mater.* **2008**, *1*, 208−226.
(3) Meyers, M. A.; Chen, P. Y.; Lin, A. Y. M.; Seki, Y. Biological Materials: Structure and Mechanical Properties. *Prog. Mater. Sci.* **2008**, *53*, 1−206.
(4) Seknazi, E.; Pokroy, B. Residual Strain and Stress in Biocrystals. *Adv. Mater.* **2018**, *30*, No. 1707263.
(5) Kunitake, M. E.; Baker, S. P.; Estroff, L. A. The Effect of Magnesium Substitution on the Hardness of Synthetic and Biogenic Calcite. *MRS Commun.* **2012**, *2*, 113−116.
(6) Bianco-Stein, N.; Polishchuk, I.; Lang, A.; Portal, L.; Dejoie, C.; Pokroy, B. High-Mg Calcite Nanoparticles Within a Low-Mg Calcite Matrix via Spinodal Decomposition: A Widespread Phenomenon in Biomineralization **2021** *119* e2120177119 DOI: 10.1073/pnas.2120177119.
(7) Bianco-Stein, N.; Polishchuk, I.; Lang, A.; Atiya, G.; Villanova, J.; Zaslansky, P.; Katsman, A.; Pokroy, B. Structural and Chemical Variations in Mg-Calcite Skeletal Segments of Coralline Red Algae Lead to Improved Crack Resistance. *Acta Biomater.* **2021**, *130*, 362−373.
(8) Broad, A.; Ford, I. J.; Duffy, D. M.; Darkins, R. Magnesium-Rich Nanoprecipitates in Calcite: Atomistic Mechanisms Responsible for Toughening in Ophiocoma Wendtii. *Phys. Chem. Chem. Phys.* **2020**, *22*, 10056−10062.
(9) Frølich, S.; Sørensen, H. O.; Hakim, S. S.; Marin, F.; Stipp, S. L. S.; Birkedal, H. Smaller Calcite Lattice Deformation Caused by Occluded Organic Material in Coccoliths than in Mollusk Shell. *Cryst. Growth Des.* **2015**, *15*, 2761−2767.
(10) Pokroy, B.; Fitch, A.; Zolotoyabko, E. The Microstructure of Biogenic Calcite: A View by High-Resolution Synchrotron Powder Diffraction. *Adv. Mater.* **2006**, *18*, 2363−2368.
(11) Pokroy, B.; Fitch, A. N.; Marin, F.; Kapon, M.; Adir, N.; Zolotoyabko, E. Anisotropic Lattice Distortions in Biogenic Calcite Induced by Intra-Crystalline Organic Molecules. *J. Struct. Biol.* **2006**, *155*, 96−103.
(12) Herman, A.; Addadi, L.; Weiner, S. Interactions of Sea-Urchin Skeleton Macromolecules with Growing Calcite Crystals— a Study of Intracrystalline Proteins. *Nature* **1988**, *331*, 546−548.
(13) Berman, A.; Addadi, L.; Kvick, A.; Leiserowitz, L.; Nelson, M.; Weiner, S. Intercalation of Sea Urchin Proteins in Calcite: Study of a Crystalline Composite Material. *Science* **1990**, *250*, 664−667.
(14) Munch, E.; Launey, M. E.; Alsem, D. H.; Saiz, E.; Tomsia, A. P.; Ritchie, R. O. Tough, Bio-Inspired Hybrid Materials. *Science* **2008**, *322*, 1516−1520.
(15) Nudelman, F.; Sommerdijk, N. A. J. M. Biomineralization as an Inspiration for Materials Chemistry. *Angew. Chem., Int. Ed.* **2012**, *51*, 6582−6596.
(16) Borukhin, S.; Bloch, L.; Radlauer, T.; Hill, A. H.; Fitch, A. N.; Pokroy, B. Screening the Incorporation of Amino Acids into an Inorganic Crystalline Host: The Case of Calcite. *Adv. Funct. Mater.* **2012**, *22*, 4216−4224.
(17) Mijowska, S.; Polishchuk, I.; Lang, A.; Seknazi, E.; Dejoie, C.; Fermani, S.; Falini, G.; Demitri, N.; Polentarutti, M.; Katsman, A.; Pokroy, B. High Amino Acid Lattice Loading at Nonambient Conditions Causes Changes in Structure and Expansion Coefficient of Calcite. *Chem. Mater.* **2020**, *32*, 4205−4212.
(18) Seknazi, E.; Mijowska, S.; Polishchuk, I.; Pokroy, B. Incorporation of Organic and Inorganic Impurities into the Lattice of Metastable Vaterite. *Inorg. Chem. Front.* **2019**, *6*, 2696−2703.
(19) Lang, A.; Mijowska, S.; Polishchuk, I.; Fermani, S.; Falini, G.; Katsman, A.; Marin, F.; Pokroy, B. Acidic Monosaccharides Become Incorporated into Calcite Single Crystals**. *Chem. - Eur. J.* **2020**, *26*, 16860−16868.
(20) Seknazi, E.; Levy, D.; Polishchuk, I.; Katsman, A.; Pokroy, B. Experimental and Theoretical Insights into the Bioinspired Formation of Disordered Ba-Calcite. *Adv. Funct. Mater.* **2020**, *30*, No. 1805028.
(21) Kulak, A. N.; Yang, P.; Kim, Y.-Y.; Armes, S. P.; Meldrum, F. C. Colouring Crystals with Inorganic Nanoparticles. *Chem. Commun.* **2014**, *50*, 67−69.
(22) Hanisch, A.; Yang, P.; Kulak, A. N.; Fielding, L. A.; Meldrum, F. C.; Armes, S. P. Phosphonic Acid-Functionalized Diblock Copolymer Nano-Objects via Polymerization-Induced Self-Assembly: Synthesis, Characterization, and Occlusion into Calcite Crystals. *Macromolecules* **2016**, *49*, 192−204.
(23) Kulak, A. N.; Semsarilar, M.; Kim, Y.-Y.; Ihli, J.; Fielding, L. A.; Cespedes, O.; Armes, S. P.; Meldrum, F. C. One-Pot Synthesis of an Inorganic Heterostructure: Uniform Occlusion of Magnetite Nanoparticles within Calcite Single Crystals. *Chem. Sci.* **2014**, *5*, 738−743.
(24) Marzec, B.; Green, D. C.; Holden, M. A.; Coté, A. S.; Ihli, J.; Khalid, S.; Kulak, A.; Walker, D.; Tang, C.; Duffy, D. M.; Kim, Y. Y.; Meldrum, F. C. Amino Acid Assisted Incorporation of Dye Molecules within Calcite Crystals. *Angew. Chem., Int. Ed.* **2018**, *57*, 8623−8628.
(25) Estroff, L. A.; Cohen, I. Micelles in a Crystal. *Nat. Mater.* **2011**, *10*, 810−811.
(26) Ren, J.; Liu, Y.; Li, H. Incorporating Polymers within a Single-crystal: From Heterogeneous Structure to Multiple Functions. *J. Polym. Sci.* **2022**, *60*, 1151−1173.
(27) Liu, Y.; Yuan, W.; Shi, Y.; Chen, X.; Wang, Y.; Chen, H.; Li, H. Functionalizing Single Crystals: Incorporation of Nanoparticles Inside Gel-Grown Calcite Crystals. *Angew. Chem.* **2014**, *126*, 4211−4215.
(28) Li, H.; Estroff, L. A. Calcite Growth in Hydrogels: Assessing the Mechanism of Polymer-Network Incorporation into Single Crystals. *Adv. Mater.* **2009**, *21*, 470−473.
(29) Green, D. C.; Ihli, J.; Kim, Y.-Y.; Chong, S. Y.; Lee, P. A.; Empson, C. J.; Meldrum, F. C. Rapid Screening of Calcium Carbonate Precipitation in the Presence of Amino Acids: Kinetics, Structure, and Composition. *Cryst. Growth Des.* **2016**, *16*, 5174−5183.
(30) Kim, Y.-Y.; Carloni, J. D.; Demarchi, B.; Sparks, D.; Reid, D. G.; Kunitake, M. E.; Tang, C. C.; Duer, M. J.; Freeman, C. L.; Pokroy, B.; Penkman, K.; Harding, J. H.; Estroff, L. A.; Baker, S. P.; Meldrum, F. C. Tuning Hardness in Calcite by Incorporation of Amino Acids. *Nat. Mater.* **2016**, *15*, 903−910.
(31) Alberts, B.; Johnson, A.; Lewis, J.; Morgan, D.; Raff, M.; Roberts, K.; Walter, P. *Molecular Biology of the Cell*; GARLAND PUB: USA, 2017.
(32) Gibbs, D.; Lohrmann, R.; Orgel, L. E. Template-Directed Synthesis and Selective Adsorption of Oligoadenylates on Hydroxyapatite. *J. Mol. Evol.* **1980**, *15*, 347−354.
(33) James Cleaves, H.; Crapster-Pregont, E.; Jonsson, C. M.; Jonsson, C. L.; Sverjensky, D. A.; Hazen, R. A. The Adsorption of Short Single-Stranded DNA Oligomers to Mineral Surfaces. *Chemosphere* **2011**, *83*, 1560−1567.
(34) Grunenwald, A.; Keyser, C.; Sautereau, A. M.; Crubézy, E.; Ludes, B.; Drouet, C. Adsorption of DNA on Biomimetic Apatites: Toward the Understanding of the Role of Bone and Tooth Mineral on the Preservation of Ancient DNA. *Appl. Surf. Sci.* **2014**, *292*, 867−875.
(35) Sarhan, M. S.; Lehmkuhl, A.; Straub, R.; Tett, A.; Wieland, G.; Francken, M.; Zink, A.; Maixner, F. Ancient DNA Diffuses from Human Bones to Cave Stones. *iScience* **2021**, *24*, No. 103397.
(36) Goring, C. A. I.; Bartholomew, Wv. ADSORPTION OF MONONUCLEOTIDES, NUCLEIC ACIDS, AND NUCLEOPROTEINS BY CLAYS. *Soil Sci.* **1952**, *74*, 149−164.
(37) Ferris, J. P.; Ertem, G.; Agarwal, V. K. The Adsorption of Nucleotides and Polynucleotides on Montmorillonite Clay. *Origins Life Evol. Biosphere* **1989**, *19*, 153−164.
(38) Ferris, J. P. Mineral Catalysis and Prebiotic Synthesis: Montmorillonite-Catalyzed Formation of RNA. *Elements* **2005**, *1*, 145−149.
(39) Ferris, J. P.; Hill, A. R.; Liu, R.; Orgel, L. E. Synthesis of Long Prebiotic Oligomers on Mineral Surfaces. *Nature* **1996**, *381*, 59−61.

https://doi.org/10.1021/acs.cgd.3c00367
Cryst. Growth Des. 2023, 23, 5117−5125

(40) Franchi, M.; Bramanti, E.; Bonzi, L. M.; Orioli, P. L.; Vettori, C.; Gallori, E. CLAY-NUCLEIC ACID COMPLEXES: CHARACTERISTICS AND IMPLICATIONS FOR THE PRESERVATION OF GENETIC MATERIAL IN PRIMEVAL HABITATS. 1997 DOI: 10.1023/A:1006557832574.
(41) Tuross, N. The Biochemistry of Ancient DNA in Bone. *Experientia* **1994**, *50*, 530−535.
(42) Collins, M. J.; Nielsen-Marsh, C. M.; Hiller, J.; Smith, C. I.; Roberts, J. P.; Prigodich, Rv.; Wess, T. J.; Csapo, J.; Millard, A. R.; Turner-Walker, G. The Survival of Organic Matter in Bone: A Review. *Archaeometry* **2002**, *44*, 383−394.
(43) Keil, R. G.; Montluçon, D. B.; Prahl, F. G.; Hedges, J. I. Sorptive Preservation of Labile Organic Matter in Marine Sediments. *Nature* **1994**, *370*, 549−552.
(44) Delabarde, T.; Keyser, C.; Tracqui, A.; Charabidze, D.; Ludes, B. The Potential of Forensic Analysis on Human Bones Found in Riverine Environment. *Forensic Sci. Int.* **2013**, *228*, e1−e5.
(45) Könnyű, B.; Czárán, T.; Szathmáry, E. Prebiotic Replicase Evolution in a Surface-Bound Metabolic System: Parasites as a Source of Adaptive Evolution. *BMC Evol. Biol.* **2008**, *8*, 267.
(46) Orgel, L. E. The Origin of Life—a Review of Facts and Speculations. *Trends Biochem. Sci.* **1998**, *23*, 491−495.
(47) Otroshchenko, V. A.; Vasilyeva, Nv. The Role of Mineral Surfaces in the Origin of Life. *Origins Life Evol. Biosphere* **1977**, *8*, 25−31.
(48) Shen, M.; Jiao, K.; Wang, C.; Ehrlich, H.; Wan, M.; Hao, D.; Li, J.; Wan, Q.; Tonggu, L.; Yan, J.; Wang, K.; Ma, Y.; Chen, J.; Tay, F. R.; Niu, L. Extracellular DNA: A Missing Link in the Pathogenesis of Ectopic Mineralization. *Adv. Sci.* **2022**, *9*, No. 2103693.
(49) Ivanova, L. A.; Egorov, V. V.; Zabrodskaya, Y. A.; Shaldzhyan, A. A.; Baranchikov, A. Ye.; Tsvigun, N. V.; Lykholay, A. N.; Yapryntsev, A. D.; Lebedev, D. V.; Kulminskaya, A. A. Matrix Is Everywhere: Extracellular DNA Is a Link between Biofilm and Mineralization in Bacillus Cereus Planktonic Lifestyle. *NPJ Biofilms Microbiomes* **2023**, *9*, No. 9.
(50) Orriss, I. R.; Utting, J. C.; Brandao-Burch, A.; Colston, K.; Grubb, B. R.; Burnstock, G.; Arnett, T. R. Extracellular Nucleotides Block Bone Mineralization in Vitro: Evidence for Dual Inhibitory Mechanisms Involving Both P2Y2 Receptors and Pyrophosphate. *Endocrinology* **2007**, *148*, 4208−4216.
(51) Zhao, D.; Wang, C.-Q.; Zhuo, R.-X.; Cheng, S.-X. Modification of Nanostructured Calcium Carbonate for Efficient Gene Delivery. *Colloids Surf., B* **2014**, *118*, 111−116.
(52) Chen, S.; Zhao, D.; Li, F.; Zhuo, R.-X.; Cheng, S.-X. Co-Delivery of Genes and Drugs with Nanostructured Calcium Carbonate for Cancer Therapy. *RSC Adv.* **2012**, *2*, No. 1820.
(53) Maleki Dizaj, S.; Barzegar-Jalali, M.; Zarrintan, M. H.; Adibkia, K.; Lotfipour, F. Calcium Carbonate Nanoparticles as Cancer Drug Delivery System. *Expert Opin. Drug Delivery* **2015**, *12*, 1649−1660.
(54) Wang, C.-Q.; Gong, M.-Q.; Wu, J.-L.; Zhuo, R.-X.; Cheng, S.-X. Dual-Functionalized Calcium Carbonate Based Gene Delivery System for Efficient Gene Delivery. *RSC Adv.* **2014**, *4*, 38623−38629.
(55) Cheng, B.; Cai, W.; Yu, J. DNA-Mediated Morphosynthesis of Calcium Carbonate Particles. *J. Colloid Interface Sci.* **2010**, *352*, 43−49.
(56) Athanasiadou, D.; Carneiro, K. M. M. DNA Nanostructures as Templates for Biomineralization. *Nat. Rev. Chem.* **2021**, *5*, 93−108.
(57) Lukeman, P. S.; Stevenson, M. L.; Seeman, N. C. Morphology Change of Calcium Carbonate in the Presence of Polynucleotides. *Cryst. Growth Des.* **2008**, *8*, 1200−1202.
(58) Colon, S.; Paige, A.; Bolarinho, R.; Young, H.; Gerdon, A. E. Secondary Structure of DNA Aptamer Influences Biomimetic Mineralization of Calcium Carbonate. *ACS Appl. Mater. Interfaces* **2023**, *15*, 6274−6282.
(59) Sommerdijk, N. A. J. M.; van Leeuwen, E. N. M.; Vos, M. R. J.; Jansen, J. A. Calcium Carbonate Thin Films as Biomaterial Coatings Using DNA as Crystallization Inhibitor. *CrystEngComm* **2007**, *9*, No. 1209.
(60) Soukup, G. A. Nucleic Acids: General Properties. In *eLS*; Wiley, 2003 DOI: 10.1038/npg.els.0001335.
(61) Borisov, S. V.; Magarill, S. A.; Pervukhina, Nv. CRYSTALLOGRAPHIC ANALYSIS OF THREE MODIFICATIONS OF CaCO3: CALCITE, ARAGONITE, VATERITE. *J. Struct. Chem.* **2021**, *62*, 1027−1037.
(62) de Leeuw, N. H.; Parker, S. C. Surface Structure and Morphology of Calcium Carbonate Polymorphs Calcite, Aragonite, and Vaterite: An Atomistic Approach. *J. Phys. Chem. B* **1998**, *102*, 2914−2922.
(63) Konopacka-Łyskawa, D. Synthesis Methods and Favorable Conditions for Spherical Vaterite Precipitation: A Review. *Crystals* **2019**, *9*, No. 223.
(64) Hood, M. A.; Landfester, K.; Muñoz-Espí, R. The Role of Residue Acidity on the Stabilization of Vaterite by Amino Acids and Oligopeptides. *Cryst. Growth Des.* **2014**, *14*, 1077−1085.
(65) Njegić-Džakula, B.; Falini, G.; Brečević, L.; Skoko, Ž.; Kralj, D. Effects of Initial Supersaturation on Spontaneous Precipitation of Calcium Carbonate in the Presence of Charged Poly-l-Amino Acids. *J. Colloid Interface Sci.* **2010**, *343*, 553−563.
(66) Hou, W.; Feng, Q. Morphology and Formation Mechanism of Vaterite Particles Grown in Glycine-Containing Aqueous Solutions. *Mater. Sci. Eng.: C* **2006**, *26*, 644−647.
(67) Chuajiw, W.; Takatori, K.; Igarashi, T.; Hara, H.; Fukushima, Y. The Influence of Aliphatic Amines, Diamines, and Amino Acids on the Polymorph of Calcium Carbonate Precipitated by the Introduction of Carbon Dioxide Gas into Calcium Hydroxide Aqueous Suspensions. *J. Cryst. Growth* **2014**, *386*, 119−127.
(68) Iqbal, M. J.; Riaz, M. S.; Talha, K.; Shoukat, R.; Mahmood, S.; Ammar, M.; Li, H. Synthesis and Transformation of Calcium Carbonate Polymorphs with Chiral Purine Nucleotides. *New J. Chem.* **2022**, *46*, 22612−22620.
(69) Xiang, L.; Kong, W.; Su, J.; Liang, J.; Zhang, G.; Xie, L.; Zhang, R. Amorphous Calcium Carbonate Precipitation by Cellular Biomineralization in Mantle Cell Cultures of Pinctada Fucata. *PLoS One* **2014**, *9*, No. e113150.
(70) Rodriguez-Blanco, J. D.; Shaw, S.; Benning, L. G. How to Make 'Stable' ACC: Protocol and Preliminary Structural Characterization. *Mineral. Mag.* **2008**, *72*, 283−286.
(71) Shaked, H.; Polishchuk, I.; Nagel, A.; Bekenstein, Y.; Pokroy, B. Long-Term Stabilized Amorphous Calcium Carbonate—an Ink for Bio-Inspired 3D Printing. *Mater. Today Bio* **2021**, *11*, No. 100120.
(72) Mehta, N.; Gaëtan, J.; Giura, P.; Azaïs, T.; Benzerara, K. Detection of Biogenic Amorphous Calcium Carbonate (ACC) Formed by Bacteria Using FTIR Spectroscopy. *Spectrochim. Acta, Part A* **2022**, *278*, No. 121262.
(73) Weir, C. E.; Lippincott, E. R. Infrared Studies of Aragonite, Calcite, and Vaterite Type Structures in the Borates, Carbonates, and Nitrates. *J. Res. Natl. Bur. Stand., Sect. A* **1961**, *65A*, No. 173.
(74) Shechter, A.; Glazer, L.; Cheled, S.; Mor, E.; Weil, S.; Berman, A.; Bentov, S.; Aflalo, E. D.; Khalaila, I.; Sagi, A. A Gastrolith Protein Serving a Dual Role in the Formation of an Amorphous Mineral Containing Extracellular Matrix. 2008 DOI: 10.1073/pnas.080019310.
(75) Aizenberg, J.; Addadi, L.; Weiner, S.; Lambert, G. Stabilization of Amorphous Calcium Carbonate by Specialized Macromolecules in Biological and Synthetic Precipitates. *Adv. Mater.* **1996**, *8*, 222−226.
(76) Addadi, L.; Raz, S.; Weiner, S. Taking Advantage of Disorder: Amorphous Calcium Carbonate and Its Roles in Biomineralization. *Adv. Mater.* **2003**, *15*, 959−970.
(77) Bentov, S.; Weil, S.; Glazer, L.; Sagi, A.; Berman, A. Stabilization of Amorphous Calcium Carbonate by Phosphate Rich Organic Matrix Proteins and by Single Phosphoamino Acids. *J. Struct. Biol.* **2010**, *171*, 207−215.
(78) Zou, Z.; Yang, X.; Albéric, M.; Heil, T.; Wang, Q.; Pokroy, B.; Politi, Y.; Bertinetti, L. Additives Control the Stability of Amorphous Calcium Carbonate via Two Different Mechanisms: Surface Adsorption versus Bulk Incorporation. *Adv. Funct. Mater.* **2020**, *30*, No. 2000003.

(79) Christy, A. G. A Review of the Structures of Vaterite: The Impossible, the Possible, and the Likely. *Cryst. Growth Des.* **2017**, *17*, 3567−3578.
(80) Kabalah-Amitai, L.; Mayzel, B.; Kauffmann, Y.; Fitch, A. N.; Bloch, L.; Gilbert, P. U. P. A.; Pokroy, B. Vaterite Crystals Contain Two Interspersed Crystal Structures. *Science* **2013**, *340*, 454−457.
(81) Kamhi, S. R. On the Structure of Vaterite CaCO3. *Acta Crystallogr.* **1963**, *16*, 770−772.
(82) Zolotoyabko, Emil.; Sons, J. W. *Basic Concepts of X-Ray Diffraction*; Wiley-VCH: Weinheim, 2014.
(83) Zolotoyabko, E.; Quintana, J. P. Non-Destructive Microstructural Analysis with Depth Resolution: Application to Seashells. *J. Appl. Crystallogr.* **2002**, *35*, 594−599.
(84) Avaro, J. T.; Ruiz-Agudo, C.; Landwehr, E.; Hauser, K.; Gebauer, D. Impurity-Free Amorphous Calcium Carbonate, a Preferential Material for Pharmaceutical and Medical Applications. *Eur. J. Mineral.* **2019**, *31*, 231−236.
(85) Marsh, M. E.; Sass, R. L. Phosphoprotein Particles: Calcium and Inorganic Phosphate Binding Structures. *Biochemistry* **1984**, *23*, 1448−1456.
(86) Marsh, M. E. Binding of Calcium and Phosphate Ions to Dentin Phosphophoryn. *Biochemistry* **1989**, *28*, 346−352.
(87) Wilson, J. E.; Chin, A. Chelation of Divalent Cations by ATP, Studied by Titration Calorimetry. *Anal. Biochem.* **1991**, *193*, 16−19.
(88) HOLM, N. G. The Significance of Mg in Prebiotic Geochemistry. *Geobiology* **2012**, *10*, 269−279.
(89) Clarke, K.; Kashiwaya, Y.; King, M. T.; Gates, D.; Keon, C. A.; Cross, H. R.; Radda, G. K.; Veech, R. L. The β/α Peak Height Ratio of ATP. *J. Biol. Chem.* **1996**, *271*, 21142−21150.
(90) Katsifaras, A.; Spanos, N. Effect of Inorganic Phosphate Ions on the Spontaneous Precipitation of Vaterite and on the Transformation of Vaterite to Calcite. *J. Cryst. Growth* **1999**, *204*, 183−190.
(91) Ishikawa, M.; Ichikuni, M. Coprecipitation of Phosphate with Calcite. *Geochem. J.* **1981**, *15*, 283−288.
(92) Suzuki, T.; Inomata, S.; Sawada, K. Adsorption of Phosphate on Calcite. *J. Chem. Soc., Faraday Trans. 1* **1986**, *82*, No. 1733.
(93) Sawada, K.; Yoshida, S.; Suzuki, T. Adsorption of Phosphate on Vaterite. *J. Chem. Soc., Faraday Trans.* **1992**, *88*, No. 2227.
(94) Kennard, O.; Isaacs, N. W.; Motherwell, W. D. S.; Coppola, J. C.; Wampler, D. L.; Larson, A. C.; Watson, D. G. The Crystal and Molecular Structure of Adenosine Triphosphate. *Proc. R. Soc. London, Ser. A* **1971**, *325*, 401−436.
(95) Lang, A.; Brif, A.; Polishchuk, I.; Fitch, A. N.; Feldmann, J.; Pokroy, B. Excessive Increase in the Optical Band Gap of Near-Infrared Semiconductor Lead (II) Sulfide via the Incorporation of Amino Acids. *Adv. Opt. Mater.* **2022**, *10*, No. 2200203.
(96) Shannon, R. D. Revised Effective Ionic Radii and Systematic Studies of Interatomic Distances in Halides and Chalcogenides. *Acta Crystallogr., Sect. A* **1976**, *32*, 751−767.
(97) Liao, J.-C.; Sun, S.; Chandler, D.; Oster, G. The Conformational States of Mg*ATP in Water. *Eur. Biophys. J.* **2004**, *33*, 29−37.
(98) Pokroy, B.; Falini, G.; Polishchuk, I.; Portal, L.; Zilberberg, R. DNA and RNA Incorporation into Minerals: From Origin of Life to Gene Therapy.
(99) Scardi, P. Diffraction Line Profiles in the Rietveld Method. *Cryst. Growth Des.* **2020**, *20*, 6903−6916.
(100) Rietveld, H. M. A Profile Refinement Method for Nuclear and Magnetic Structures. *J. Appl. Crystallogr.* **1969**, *2*, 65−71.
(101) Toby, B. H.; von Dreele, R. B. GSAS-II: The Genesis of a Modern Open-Source All Purpose Crystallography Software Package. *J. Appl. Crystallogr.* **2013**, *46*, 544−549.

https://doi.org/10.1021/acs.cgd.3c00367
Cryst. Growth Des. 2023, 23, 5117−5125